Peak Alpine metamorphic conditions from staurolite bearing metapelites in the Monte Rosa nappe (Central European Alps) and geodynamic implications

Joshua D Vaughan-Hammon, Cindy Luisier, Lukas P Baumgartner, Stefan M Schmalholz

MR. JOSHUA DAVID VAUGHAN-HAMMON (Orcid ID : 0000-0002-0388-146X)

Article type : Original Article

Peak Alpine metamorphic conditions from staurolite bearing metapelites in the Monte Rosa nappe (Central European Alps) and geodynamic implications

Joshua D. Vaughan-Hammon[1], Cindy Luisier[1,2], Lukas P. Baumgartner[1], Stefan M. Schmalholz[1]

[1] Institute of Earth Sciences, University of Lausanne, Lausanne 1015, Switzerland,

[2] Université de Rennes, CNRS, Géosciences Rennes UMR 6118, Rennes, France

Correspondence:

Joshua D. Vaughan-Hammon, Institute of Earth Sciences, University of Lausanne, Lausanne 1015, Switzerland. Email: Joshua.vaughan-hammon@unil.ch

This article has been accepted for publication and undergone full peer review but has not been through the copyediting, typesetting, pagination and proofreading process, which may lead to differences between this version and the Version of Record. Please cite this article as doi: 10.1111/JMG.12595

ABSTRACT

The tectono-metamorphic evolution of the European Alps is still contentious. The Monte Rosa tectonic unit is a prominent nappe in the Central European Alps and estimates of its peak Alpine pressure (P) and temperature (T) conditions are essential for reconstructing its tectono-metamorphic evolution. However, the reported peak Alpine P and T estimates vary considerably between 1.2 and 2.7 GPa and 490 and 640 °C for a variety of lithologies.

Here, we show petrology and pseudosection modelling of metapelitic assemblages from the western portions of the Monte Rosa nappe (upper Ayas valley, Italy). We present newly discovered staurolite-chloritoid bearing metapelitic assemblages. These assemblages exhibit an Alpine high-P metamorphic overprint of a former contact-metamorphic mineral assemblage generated by post-Variscan granitic intrusions. Staurolite contains major amounts of Zn (up to 1.0 atoms per formula units), which is currently, in contrast to Fe- and Mg-staurolite end-members, not considered in any thermodynamic database. We employ two end-member mixing models for Zn in staurolite, site mixing and molecular mixing. Both models enlarge the P and T stability range for the observed assemblage, where site mixing has the largest influence of ± 0.2 GPa and ± 20 °C. Our results for three metapelite assemblages, with and without staurolite, indicate peak Alpine P of 1.6 ± 0.2 GPa and peak T of 585 ± 20 °C. These peak P estimates agree with previously published estimates for metagranites in the nappe, and are in stark contrast with peak P obtained from talc, chloritoid, phengite and quartz bearing lithologies termed ‘whiteschists’ (>2.2 GPa). Our results confirm a variation of peak Alpine P of 0.6 ± 0.2 GPa between metagranite/metapelite lithologies and a nearby whiteschist lens (>2.2 GPa) within the metagranite. Field observations indicate that the studied region is structurally coherent and that the whiteschist is not a tectonic slice formed by tectonic mélange. We suggest that the consistent peak P for metapelite and metagranite assemblages represents the regional peak P and that the higher pressure recorded in the whiteschist lens is likely due to dynamic pressure, possibly resulting from tectonic and/or reaction-induced stresses. If the calculated P of 1.6 ± 0.2 GPa represents regional peak Alpine conditions, then the Monte Rosa nappe was exhumed from a significantly shallower depth than previously assumed, based on peak P estimates >2.2 GPa for whiteschist lithologies.

KEYWORDS

Central European Alps, metapelite, high-pressure metamorphism, Zn-staurolite, tectonic pressure

1 INTRODUCTION

The Western and Central European Alps (Figure 1) played a significant role in the pioneering discoveries of high- and ultra high-pressure, (U)HP, metamorphic rocks (Chopin, 1987; Chopin et al., 1991; Chopin and Monié, 1984; Goffe and Chopin, 1986; Reinecke, 1991). These rocks contain evidence of the geodynamic environment of orogens and provide insight into pressures, temperatures and chemical systems unobservable to humans. Geographically, the Monte Rosa nappe is located in the Central European Alps. It is a continental unit belonging to the Middle Penninic domain generated during the western Alpine orogeny (Figure 1; e.g. Handy et al. (2010)), that underwent HP conditions associated with its burial below the Adriatic continent during the orogenesis. Petrological investigations into rare magnesiochloritoid-bearing lithologies (named 'whiteschists') revealed Alpine eclogite facies metamorphic conditions (Chopin and Monié, 1984). These discoveries prompted numerous studies assessing suitable mechanisms by which (U)HP crustal rocks can be transported during orogenesis to and from significant depth; sometimes more than 100 km if lithostatic pressure is assumed (Hacker and Gerya, 2013; Kurz and Froitzheim, 2002). However, published estimates of peak Alpine metamorphic conditions for the Monte Rosa nappe highlight large disparities; with peak P estimates ranging between 1.2 and 2.7 GPa and temperature (T) estimates between 490 and 640 ºC (Figure 2a) (Borghi et al., 1996; Chopin and Monié, 1984; Dal Piaz and Lombardo, 1986; Ferrando et al., 2002; Gasco et al., 2011; Keller et al., 2004; Lapen et al., 2007; Le Bayon et al., 2006; Luisier et al., 2019).

The assessment of suitable mechanisms by which rocks can be transported through an orogen from (U)HP conditions to the surface requires an estimate of the maximal burial depth at which they equilibrated (e.g. Petrini and Podladchikov, 2000). Large disparities in peak P within a structurally coherent nappe poses difficulties when attempting to resolve the tectono-metamorphic history if it is assumed that peak P represents the lithostatic pressure, which is mainly a function of burial depth (Schenker et al., 2015; Schmalholz and Podladchikov, 2014). However, the pressure, or mean stress, in a rock cannot be exactly lithostatic during an orogeny due to differential stresses, required to drive rock deformation (Gerya, 2015; Mancktelow, 1993; Mancktelow, 1995; Mancktelow, 2008; Schmalholz and Podladchikov, 2013) or to balance lateral variations in gravitational potential energy (Molnar and Lyon-Caen, 1988; Schmalholz et al., 2019; Schmalholz et al., 2014). The deviation from lithostatic pressure is commonly termed tectonic pressure and both its magnitude (Li et al., 2010; Luisier et al., 2019; Reuber et al., 2016) and impact on metamorphic reactions is disputed (Moulas et al., 2019; Wheeler, 2018).

For the Monte Rosa nappe, specifically within the western portions of the nappe at the head of the Ayas valley, Italy (Figure 2a), recent work by Luisier et al. (2019) reported peak Alpine P variations (0.8 ± 0.3 GPa) between a whiteschist (~ 2.2 GPa) and the host metagranite (~ 1.4 GPa) (Figure 2b). Based on field and microstructural observations, as well as geochemical analyses, Luisier et al. (2019) proposed that the pressure variations cannot be explained by tectonic mixing (mélange), as the whiteschist and metagranite are structurally coherent (documented by cross-cutting post-Variscan dikes). They also excluded complete retrogression of the jadeite-free metagranite and sluggish kinetics due to low water activity. Luisier et al. (2019) suggests that these peak P variations could represent tectonic pressure variations.

Here, we test whether the whiteschist HP imprint of 2.2 to 2.5 GPa represents regional, 'whole-nappe', metamorphic conditions or local deviations, within the upper Ayas valley region (Figure 2a). We have investigated numerous metapelitic samples from the Monte Rosa basement metasediments, and identified three independent mineral assemblages that are from outcrops structurally continuous with the localities of previous studies (Chopin and Monié, 1984; Luisier et al., 2019; Marger et al., 2019; Pawlig and Baumgartner, 2001). The samples are unique mineral assemblages representing peak Alpine conditions within pseudomorphs of former contact metamorphic minerals, suitable therefore, to understand further the nature and existence of peak P variations. The main assemblages we have investigated are staurolite-chloritoid bearing that are, to the best of our knowledge, the first described occurrences in the Monte Rosa nappe. Staurolite bearing assemblages can pose difficulties in thermodynamic modelling, due to the apparent compositional variability (e.g. Hawthorne et al., 1993). This variability is primarily the result of unknown site occupations involving Al, Mg, Fe^{2+}, Fe^{3+}, Ti, Cr, Zn, Co and Li, as well as H content (Dutrow et al., 1986; Griffen, 1981; Hawthorne et al., 1993; Holdaway et al., 1986; Tuisku et al., 1987). These variabilities, combined with the lack of thermodynamic data for staurolite, require consideration when calculating metamorphic conditions of formation, specifically when applying the appropriate mixing model (e.g. Berman, 1990; Powell and Holland, 1993). For the analyzed rocks, we investigate different mixing models and the subsequent effects on pseudosection derived peak P and T.

2 GEOLOGICAL SETTING

2.1 General overview

The Monte Rosa massif, christened the "Queen of the Alps" (King, 1858), is one of the geologically most studied tectonic units in the Alpine orogenic chain (Dal Piaz, 2001). It belongs to the internal crystalline massifs of the Western and Central Alps, along with the Dora Maira and Gran Paradiso massifs (Figure 1a). These massifs represent dismembered continental crust incorporated into the Eocene-aged Alpine orogeny (Steck et al., 2015). The Monte Rosa massif consists of a pre-Variscan basement, which was intruded by Permian-age granitic bodies (Figure 2a). The current position of the basement complex resides within the collisional Austroalpine-Penninic wedge and lies structurally between the overlying Zermatt-Saas and underlying Antrona ophiolitic sequences (Figure 1b).

The palaeogeographic location of the Monte Rosa unit has been attributed in many earlier studies to the southern Briançonnais domain as part of the European margin (Dal Piaz, 2001; Steck et al., 2015). This domain was separated from the European margin by the Valais basin to the north and bordered by the Piemont basin to the south prior to their subsequent collision during Alpine orogeny.

The Monte Rosa massif consists of lithologies that record a multiphase metamorphic history. This massif was described as a complex poly-metamorphic basement by Bearth (1952), consisting of high grade deformed paragneisses and a younger granitic complex, consisting of granitic to granodioritic intrusions and associated dykes. The pre-granitic polymetamorphic basement complex contains metapelites locally preserving a high grade relict assemblage composed of garnet, biotite, sillimanite, quartz, K-feldspar, cordierite, muscovite and plagioclase (Bearth, 1952; Dal Piaz and Lombardo, 1986). Subsequent petrological investigations of these assemblages revealed a high-temperature, pre-Alpine assemblage related to an upper Amphibolite facies sillimanite-K-feldspar metamorphism, ~ 700 ºC/ 0.3-0.6 GPa (Ferrando et al., 2002), associated with Variscan metamorphism and dated at c. 330 Ma (e.g. Engi et al., 2001). This basement complex was folded and deformed prior to the post-Variscan granitic intrusions dated at 269 ± 4 Ma (Pawlig, 2001). A contact aureole in the metasediments of the basement complex resulted from the thermal perturbation related to the granitic intrusions, leading locally to partial melting (Dal Piaz, 2001) (S1 supplementary material, herein referred to as SM-S*(n)*). Hydrothermal alteration locally overprinting the granite has been documented (Luisier et al., 2019; Marger et al., 2019; Pawlig and Baumgartner, 2001). Th e Alpine HP eclogite facies

metamorphism (1.2-2.7 GPa / 490-640 ºC (Borghi et al., 1996; Chopin and Monié, 1984; Dal Piaz and Lombardo, 1986; Ferrando et al., 2002; Gasco et al., 2011; Keller et al., 2004; Lapen et al., 2007; Le Bayon et al., 2006)) has been dated at 42.6 ± 0.6 Ma (Lapen et al., 2007) and retrogression to greenschist facies was dated between 40-37 Ma for both the Monte Rosa (Chopin and Monié, 1984) and the overlying Zermatt-Saas units (Skora et al., 2015). Lastly, the Monte Rosa nappe exhibits an albite-oligoclase metamorphic isograd first described by Bearth (1958). This Barrovian-style isograd is similar to other units of the Central Alps (e.g. Lepontine Dome), and suggests a post-peak Alpine regional thermal metamorphic event (Niggli, 1960). Fission track zircon ages indicate that the western region of the Monte Rosa nappe cooled below ~ 225 °C at c. 33 Ma (Hurford et al., 1991). Hence, the massif was exhumed to a depth less than ~ 10 km already at c. 33 Ma, assuming a geothermal gradient of 22.5 °C/km.

2.2 Previous estimates of peak Alpine PT

We review shortly previous estimates for peak Alpine conditions incurred by basement lithologies of the Monte Rosa nappe, focusing on its western portions, namely the upper Ayas and Gressoney valleys in the southwest portions of the nappe and the Mattmark and Loranco localities (Figure 2a). The western portion of the Monte Rosa nappe is separated from the eastern portion by a structural discontinuity, termed the Stellihorn shear zone (Figure 2a, Steck et al., 2015).

Dal Piaz and Lombardo (1986) described micaschist and metabasalt samples from the upper Gressoney valley (Figure 2a). Micaschist peak HP paragenesis consists of Ph, Cld, Grt, Ky ± Gln (mineral abbreviations after Whitney and Evans (2010)). Metabasaltic peak paragenesis consists of Grt, Omp, Gln, Rt, Pg ± Qz ± Zo. Peak P was constrained at 1.4 GPa due to the absence of jadeite within the metagranite via the reaction $Ab = Jd + Qz$ (Dal Piaz and Lombardo, 1986; Holland, 1979). The minimum P was estimated at 0.8-1.0 GPa, using jadeite and omphacite molar contents of pyroxene within metabasalt samples (Holland, 1979). Minimum temperature (T) estimates were defined by the paragonite-in reaction in metabasalts: $Lws + Ab = Pg + Qz + H_2O$ (Holland, 1979). Maximum T is constrained via the chloritoid-out reaction in micaschists: $Cld + Qz = St + Grt + H_2O$ (Rao and Johannes, 1979). Peak T ranges were refined using the garnet-clinopyroxene thermometer from Ellis and Green (1979) between 440-530 ºC.

Borghi et al. (1996) sampled metapelitic and metabasic lithologies from the upper Gressoney valley. High pressure minerals consist of Qtz, Ab, Ph, Pg, Chl, Grt, Ky, Cld, Gln, Rt

and Ep. Peak P from silica content of phengite (Massonne and Schreyer, 1987) and peak T from garnet-phengite reveal a minimum pressure of 1.3 GPa and a temperature of 546 ± 21°C.

Keller et al. (2004) examined two metapelitic samples from a continuous structural layer involved within a shear zone from the Loranco locality (Figure 2). The shear zone is interpreted to represent peak Alpine HP conditions, partially preserving pre-Alpine mineral assemblages. The HP paragenesis consists of Ph, Pg, Qz, Grt, Pl, Ky, Ilm, Rt and Tur. The resulting stability field is between 620-670 °C and 1.20-1.35 GPa, via thermodynamic modelling using Berman (1988), update 92 database, constrained also by the lack of granite anatexis (Huang and Wyllie, 1974).

Gasco et al. (2011) investigated metapelitic samples and metabasic samples from a mafic boudin within the Monte Rosa basement micaschists in the upper Gressoney valley, close to the tectonic contact with the structurally higher Zermatt-Saas unit (Figure 2). Eclogite metabasic boudins represent a mineral assemblage of Omp, Gln, Grt, Ph, Lws, Rt, and Qz, presumably equilibrated at peak conditions at 2.4-2.7 GPa and 550-570 °C (Holland and Powell (1998), update 2004). Metapelite assemblages of Ph, Pg, Grt, Chl, Ab/ Olig, Hbl, Qz, Rt, Ilm ± Bt, are interpreted to represent re-equilibration during decompression at 0.7-0.9 GPa and 550-600 °C.

Peak Alpine HP conditions have also been calculated from assemblages within the Monte Rosa metagranites known as "whiteschists", consisting of chloritoid, talc, phengite and quartz ± garnet or kyanite (Chopin and Monié, 1984; Le Bayon et al., 2006; Marger et al., 2019). A refinement of these estimates has recently been made by Luisier et al. (2019) (Figure 2b). This unique assemblage has a protolith chemistry deriving from the late magmatic metasomatic alteration of the host granite (Pawlig and Baumgartner, 2001). The peak P paragenesis indicates approximately 2.2 ± 0.2 GPa at 540-600 °C (Luisier et al., 2019). Peak Alpine conditions were also estimated for the host/protolith metagranite. Peak metamorphic assemblages consist of phengite + titanite pseudomorphs replacing biotite, as well as fine-grained pseudomorphs after plagioclase, consisting of albite + zoisite ± phengite ± garnet. These parageneses, as well as additional pressure estimates based on Si-content in phengite, combined with water activity estimates, and the lack of jadeite within the metagranite, prompted the interpretation that the metagranite never experienced pressures over 1.6 GPa (at T 540-600 °C).

2.3 Study area

We have investigated metapelitic samples in the western extent of the Monte Rosa basement in a region termed the "Cirque du Véraz" (personal communication with G. Dal Piaz) within the upper

Ayas valley, Italy (Figures 2 and 3). Due to recent glacial retreat, a newly exposed area has become accessible for detailed geological mapping and sampling (Figure 3). The field area provides an exposed section through the Monte Rosa basement complex up to the overlying Zermatt-Saas Unit. Geometrically, the study area has a domal structure with Monte Rosa metagranites residing within the core of the dome, overlain sequentially by Monte Rosa polymetamorphic basement metapelites, locally overlain by a thin layer of Furgg zone metasediments, and eventually the tectonic contact with the overlying Zermatt-Saas units. The locality is situated directly on the antiformal trace of the backfold, which pervasively affects the nappe (Steck et al., 2015) (Figures 1a and 3). High strain domains typically display late-Alpine metamorphism and deformation, equilibrated to greenschist facies during decompression (Figures 3 and 4c). The basement complex locally preserves pre-Alpine structures in low strain domains (Figure 3), whose mineral assemblages were re-equilibrated during peak Alpine metamorphism (Figures 4c and d).

Samples were obtained east of the Perazzispétz ridge (Swiss coordinates E: 2626459 N: 84117 alt: 3302m and E: 2626048 N: 83526 alt: 2920m, Figures 3 and 4). The samples consist of layered metapelites (Figures 4b and c) recording a pre-Alpine foliation. Locally, granitic dikes crosscut the foliation (Figure 4b), attesting to the pre-Alpine age of the main deformation seen in these outcrops. We report few samples of former aluminosilicate bearing contact metamorphic metapelites that were subsequently equilibrated at HP conditions (Figures 4d and SM-S2). The peak Alpine metamorphic minerals are observed within pseudomorphs replacing former larger pre-Alpine minerals (Figures 4d and SM-S3). The presence of pre-Alpine dykes crosscutting metapelite lithologies (Figures 4a and b), and migmatite textures associated with pre-Alpine granitic intrusion (SM-S1) indicate that this area represents a structurally coherent tectonic body, and not a tectonic mélange.

3 METHODOLOGY

3.1 Analytical methods

Electron probe microanalysis (EPMA) of major and minor element compositions of white mica, chloritoid, staurolite, garnet and chlorite were conducted using a JEOL JXA-8350F HyperProbe at the University of Lausanne, Switzerland. In total, quantitative analysis of 46 white mica grains (197 points), 11 chloritoid grains (149 points), 12 staurolite grains (68 points), 8 garnet grains (72 points), and 5 chlorite grains (30 points) was undertaken. The operating conditions were 15.0 kV acceleration voltage and 1.5-2.0 x 10^{-8} A, with a beam diameter of 5.0 μm. Natural minerals were used as reference materials: orthoclase (K_2O, SiO_2), andalusite (Al_2O_3), albite (Na_2O), fayalite (FeO), forsterite (MgO), tephrite (MnO), wollastonite (CaO), sphalerite (ZnO), and rutile (TiO_2). Structural formulae from Howie et al. (1992) were used for stoichiometric calculations on the basis of 11 oxygens for white mica, 8 cations for chloritoid, 12 oxygens for garnet and 13 oxygens for chlorite ($(Mg,Fe)_5Al[AlSi_3O_{10}](OH)_8$). For staurolite ($(Fe^{+2},Mg,Zn)_{3\text{-}4}(Al,Fe^{+3},Ti)_{17\text{-}18}O_{16}[(Si,Al)O_4]_8H_{3\text{-}4}$ (Deer et al., 2013)), normalization assuming $Si + Al - \frac{1}{3} Li + \frac{2}{3} Ti + Fe^{3+} = 25.55$ cations as proposed in Holdaway et al. (1991) was used, due to uncertainties in H and Fe^{3+} content.

3.2 Thermodynamic modelling

Phase diagrams were calculated using the THERIAK-DOMINO software suite (de Capitani and Brown, 1987) in combination with the Berman database (Berman 1988, 92 update). This database was chosen in order to: 1) have an internally consistent database, and 2) to accurately compare thermodynamically calculated P and T with results of the study of Luisier et al. (2019). Bulk compositions were calculated based on quantitative image analysis of equilibrium subdomains in each sample, using EPMA derived mineral compositions, along with the MATLAB© based image processing software XMapTools (Lanari et al., 2014), in the chemical system NCKFMASH (SM-S7 and S11). Solution models used are after the 92 update of Berman (1988) which include: H_2O after the HAAR equation of state (Kell et al., 1984), white mica after Massonne and Szpurka (1997), chloritoid, garnet and chlorite after the 92 update of Berman (1988), and staurolite after Nagel et al. (2002).

The current solution model data for staurolite considers only Fe and Mg-endmembers (Nagel et al., 2002). However, a wealth of literature highlights a wider range of possible staurolite endmembers (e.g. Zn (e.g. Holdaway et al., 1991)). In order to account for the lack of variability in experimentally derived endmember thermodynamic data, e.g. Zn in staurolite, we have employed a method to adjust the activity of available solid solution endmember data (Nagel et al., 2002). To do so, the activity ($\alpha_i^{reduced}$) for Mg and Fe staurolite endmembers were reduced to account for the Zn endmember (see appendix 1). The thermodynamic data of the endmember staurolites were adjusted, using two mixing models to account for the Zn-concentrations analyzed, within the JUN92B database by Berman (1988) utilized by THERIAK-DOMINO. Both models assume ideal mixing: model 1 assumes molecular mixing, while model 2 assumes site mixing. We adjust the thermodynamic properties of Fe and Mg staurolite endmembers using an entropy correction, $S_{eff}^{T0,P0} = S_{MgSt}^{T0,P0} - R\ln\left(\alpha_i^{reduced}\right)$ (see appendix 1 for full derivation). PT errors are estimated from the resulting stability fields calculated with and without the entropy correction for staurolite bearing assemblages.

4 PETROGRAPHIC DESCRIPTIONS

In order to capture peak Alpine conditions, samples were taken from within the Monte Rosa polymetamorphic basement that has experienced little to no late Alpine metamorphic and deformational overprint (Figures 3 and 4c). The two samples analyzed (16MR-17 & 19MR-33) were taken from close proximity to each other (Figure 3). These samples are metapelites, which show different mineral paragenesis due to variable protolith chemistry.

4.1 Sample 16MR-17

Sample 16MR-17 displays a weakly inherited foliation defined by an assemblage of fine-grained quartz + white mica + garnet + chlorite, wrapping around large garnet porphyroblasts, as well as domains consisting of a fine-grained assemblage of staurolite, chloritoid, phengite and paragonite (Figures 5a, b and c, and SM-S4). These fine-grained domains have a pseudomorph texture, presumably after a larger mineral, due to their sharp boundaries and regular form (Figures 5a and SM-S4). Accessory minerals are apatite, rutile, tourmaline, ilmenite, zircon and monazite. Late matrix phases consist of biotite, replacing garnet, and chlorite, partially replacing garnet and biotite (Figure 5e). Two generations of garnet exist (Figure 5b). Larger garnet porphyroblasts represent an older 1st generation Grt. A second generation of smaller garnets (2nd generation Grt) are embedded in a fine-grained matrix of white mica (phengite + paragonite, Figure 5b) and minor amounts of quartz and chlorite (Figure 5e). First generation garnets show dark dissolution-precipitation rims marked by fine inclusions of an unknown mineral (Figure 5b). These dark precipitation growth rims coincide with the smaller 2nd generation garnets, which have inclusion rich cores (Figure 5b). The schistosity defined by white mica envelops 1st generation garnets suggesting the garnet grew pre- or syn-tectonically (Figure 5b). However, 2nd generation garnets grow statically and post-tectonically with undeformed white mica (Figure 5e). 2nd generation garnet is observed to grow statically over former pressure shadows associated with 1st generation garnets (Figure 5b).

Based on textural domains, two equilibrium assemblages were defined that are interpreted to have captured peak Alpine metamorphic conditions. Assemblage 1 consists of domains of staurolite, chloritoid, phengite and paragonite, pseudomorphing former andalusite, as highlighted in Figures 5a and SM-S3. The whole pseudomorph domains after andalusite have grown statically, with un-oriented mica and staurolite twins (Figure 5c). Assemblage 2 consists of 2nd generation garnets, phengite, paragonite, chlorite and quartz (Figures 5b and e). Assemblage 1 and 2 are statically grown and therefore post-kinematic.

4.2 Sample 19MR-33

Sample 19MR-33 is texturally and petrologically similar to 16MR-17. However, no staurolite is observed in the fine-grained pseudomorph domains that characterize assemblage 1, only chloritoid is present in a matrix of phengite and paragonite (Figure 5d).

5 MINERAL CHEMISTRY

Representative compositional results for phengite, paragonite, chloritoid and staurolite in assemblage 1, as well as phengite, paragonite, garnet and chlorite in assemblage 2 of sample 16MR-17 and phengite, paragonite, chloritoid in assemblage 3 of sample 19MR-33 are displayed in Table 1. In assemblage 1, two white micas are distinguished. Phengite has Si content ranging between 3.18 to 3.25 a.p.f.u, which is correlated with an increase of the Tschermak component between 0.18 to 0.25 (Figure 6a). Phengites have a K content ranging between 0.85 and 0.91 a.p.f.u. (Figure 6c). Phengite coexists with paragonite with a Na content between 0.83 to 0.87 a.p.f.u. (Figure 6c). Chloritoid compositions are relatively richer in Fe compared to Mg, with an X_{Mg} (Mg/(Mg+Fe)) between 0.26 – 0.33. Similarly, staurolite is Fe rich, with a X_{Fe} (Fe/(Mg+Fe)) of 0.68 – 0.74 (Figure 6b). The high content of zinc is remarkable in staurolite, reaching 1.0 a.p.f.u. in some samples (Figure 6d and Table 1). No Zn was found by EPMA analysis in any other mineral.

For assemblage 2 of sample 16MR-17, two white micas are also present. Phengite has Si content ranging between 3.20 to 3.37 a.f.p.u, which correlates with an increase of the Tschermak component between 0.20 to 0.37 (Figure 6a). Notably, the highest Si contents are typically within the core of phengite and the lowest at the rim (Table 1). Compared to assemblage 1 and 3, Si content of phengite are highest in this quartz bearing assemblage. Phengites have a K content ranging between 0.85 and 0.96 a.p.f.u. (Figure 6c). Phengite coexists with paragonite with a Na content between 0.85 to 0.89 a.p.f.u. (Figure 6c). Garnet compositions are almandine rich (Figure 6d) with Fe ranging between 1.41 and 1.55 a.p.f.u. and minimal zoning is observed (SM-S10).

For assemblage 3 of sample 19MR-33, two white micas are also distinguished. Phengite has Si content ranging between 3.10 to 3.21 a.f.p.u, which correlates with an increase of the Tschermak component between 0.10 to 0.21 (Figure 6a). Phengites have a K content ranging between 0.81 and 0.88 a.p.f.u. (Figure 6c). Phengite coexist with paragonite with a Na content between 0.85 to 0.95 a.p.f.u. (Figure 6c). Chloritoid compositions are enriched in Fe (1.41 and 1.55 a.p.f.u.) compared to Mg ranging between 0.50 and 0.59 a.p.f.u. (Figure 6b).

6 PHASE PETROLOGY

Due to the minimal compositional zoning of all minerals, a pseudosection approach was used in order to calculate PT conditions at fixed bulk-rock composition. Figures 7a and b show the pseudosection results in the NKFMASH system (SiO_2-Al_2O_3-FeO-MgO-K_2O-Na_2O-H_2O) with the bulk compositions displayed for assemblage 1 (phengite + paragonite + staurolite + chloritoid). The stability field of assemblage 1 was well constrained at 1.6 ± 0.05 GPa and 605 ± 2 °C. The results for the entropy correction, due to Zn, based on a 'molecular mixing' model are presented along with Si in phengite isopleths (Figure 7a). The new stability field for this assemblage is comparatively larger, expanding towards lower temperatures and higher pressures, resulting in 1.6 ± 0.1 GPa at 600 ± 5 °C. The new stability field resulting from the 'site mixing' correction is larger than the 'molecular mixing' model and results in 1.6 ± 0.2 GPa at 585 ± 15 °C (Figure 7b). The appearance of staurolite is shifted towards lower temperatures in comparison with the results using the molecular mixing model in Figure 7a and the classical solution model. Equally, the pseudosection calculations for this assemblage predicts quartz (< 1%). However, we have not observed quartz in these staurolite – chloritoid bearing assemblages.

Representative compositional microprobe results for assemblage 2 from sample 16MR-17 are displayed in Table 1 (garnet + phengite + paragonite + chlorite). Minor zoning is observed in phengite, namely high Si-content in the core of phengites, up to 3.37 a.p.f.u (Figure 6a). Similarly, minor zoning of Ca and Mn can be observed in garnet (Table 1). Therefore, we took average compositions of Si, Ca and Mn of phengite and garnet respectively, as input for bulk rock compositions. Figure 7c shows pseudosection results in the NCKFMASH system (SiO_2-Al_2O_3-FeO-MgO-K_2O-Na_2O-CaO-H_2O). Using isopleths for the modal volume of chlorite (vol%), Xparagonite and Si in phengite (a.p.f.u.), the stability field for the observed mineral assemblage ranges from 1.3 – 1.4 GPa at ~ 575 °C (Figure 7c).

Representative composition microprobe results for assemblage 3 from sample 19MR-33 are displayed in Table 1 (phengite + paragonite + chloritoid). We observe minimal zoning in this assemblage with similar values as assemblage 1 (Ph + Pg + St + Ctd). Bulk compositions are similar to assemblage 1 with the exception of lower Zn values. The stability field for the peak paragenesis is large, spanning a wider field of pressures and temperatures (Figure 7d). At

temperatures of 575 °C, inferred from assemblage 1 and 2, pressure ranges between 1.1 and 1.6 GPa.

6 DISCUSSION

6.1 Estimating peak Alpine conditions

Due to the complexity of the polymetamorphic Monte Rosa basement, three periods of geological activity may be responsible for the formation of assemblages 1, 2 and 3, that we interpret to have formed during peak Alpine conditions. These events include (from oldest to youngest): (1) HT-LP Variscan orogenesis, (2) peak high-P Alpine orogenesis, and (3) a late Alpine thermal pulse. However, field occurrences, textural relationships and petrological investigations from this study, enable us to attribute the investigated assemblages to equilibration during peak Alpine conditions (Figure 7).

Typically, the studied assemblages occur within centimeter-sized pseudomorphs in low-strain domains (Figures 3, 4c and d, and SM-S3). These pseudomorphs occur close to the late Palaeozoic metagranite intrusion and associated basement migmatites (Figure 4b). We interpret these pseudomorphs to represent relics of former contact metamorphic andalusite that formed during granite emplacement (SM-S3). Therefore, the staurolite + chloritoid bearing assemblages post-date granite emplacement and thus post-date Variscan orogenesis. Equally, the calculated P-T results for the assemblages analyzed in this study do not agree with the older high-T and low-P metamorphism, characteristics of the Variscan orogeny. Our results of 1.6 ± 0.2 GPa and 585 ± 20 °C indicate too high pressures and too low temperatures compared with estimates of 0.3-0.6 GPa and 700 °C for Variscan metamorphism (Bearth, 1952; Dal Piaz, 2001; Dal Piaz and Lombardo, 1986; Engi et al., 2001).

Another argument for the Alpine formation of the assemblages investigated, is the apparent enrichment of Na (Table 1). This enrichment resulted in the occurrence of large volume proportions of paragonite observed (up to 30%). Similar enrichment in Na of metapelites in close proximity to intrusive bodies has been reported (e.g. Eugster, 1985). These occurrences have been attributed to host-rock interaction with late magmatic hydrothermal fluids. Evidence for post-intrusion hydrothermal activity is also observed in close proximity to our locality, namely the formation of Mg-rich sericite-chlorite schists, that are the precursory equivalent to HP 'whiteschists' within the metagranite (Luisier et al., 2019; Marger et al., 2019; Pawlig and Baumgartner, 2001). Associated with hydrothermally induced Mg-enrichment of the granite protolith, depletion of Na has be observed (Pawlig and Baumgartner, 2001). The ensuing fluid migration may have contributed to the enrichment of Na in the basement metapelites.

Previous observations of staurolite within the Monte Rosa nappe have been interpreted to be associated with the post-peak Alpine Barrovian metamorphism in the Lepontine dome, far to the East of our finding (Engi et al., 2001; Niggli, 1960; Niggli, 1970; Niggli and Niggli, 1965). This isograd exists in the far eastern extent below the Monte Rosa nappe pile in the Camugera Moncucco unit (CM), which is structurally one of the deepest unit in the Western Alps (Keller et al., 2004). Observations of relic staurolite have been reported further west from the CM and are linked possibly to a HP Alpine phase, however, no thermodynamic calculations of P and T have been made (Engi et al., 2001; Niggli, 1970; Niggli and Niggli, 1965). Until now, no observations of staurolite, to the best of our knowledge, in the Monte Rosa nappe have been made west of the Stellihorn shear zone (Figure 2a).

To place the staurolite investigated within the timeframe of the late thermal pulse may pose some difficulties. Firstly, due to the location in the far western portion of the nappe, as Frey et al. (1999) places the western portions of the Monte Rosa nappe at greenschist facies during this time. Secondly, the calculated P and T within this study have too high pressures at 1.6 ± 0.2 GPa, and even at the lowest structural levels (i.e. within the CM) these pressures would be too high, as Engi et al. (2001) calculated re-equilibration during decompression at conditions of 1.1 ± 0.12 GPa and 652 ± 41 °C.

Mineral textures and calculated metamorphic conditions in this study exclude the possibility of equilibration during: (1) Variscan orogenesis, and (3) late Alpine thermal decompression, therefore, equilibration during (2) peak Alpine conditions remains. The observed assemblages most likely equilibrated in a pressure-temperature maximum during Alpine burial. This is observed both texturally and geochemically with garnet growth, as isopleths for garnet growth increase with prograding P-T conditions. Thus, the assemblages investigated here formed during peak Alpine conditions, rather than superimposing them onto a retrogressive pathway during decompression. If these assemblages represent retrogression however, the question remains: from what assemblages did they retrogress? The only pseudomorphic textures we can observe are likely after former andalusite related to Permian-aged contact metamorphism (Figure 4d and SM-S2). However, when comparing calculated P-T equilibrium domains for both assemblage 1 and 2, there does exists a small disparity (Figure 7). Assemblage 1 has ~ 0.2 GPa higher pressures and ~ 50 °C higher temperatures. This is likely due to chlorite replacing garnet (Figure 5e) during retrogression from peak conditions recorded in the staurolite-chloritoid bearing

assemblages along with the influx of H_2O rich fluids. The presented field relations, textural observations and thermodynamic calculations suggest equilibration during peak Alpine conditions.

6.2 Sensitivity of thermodynamic mixing models: Zn in staurolite

In order to constrain a reliable Alpine peak P and T incurred by the Monte Rosa basement, the calculated thermodynamic stability fields must replicate the observed mineral textures, chemistry and modal abundances. Here we will address two caveats in our calculated pseudosections: (i) the presence of Zn in staurolite in assemblage 1, and (ii) the calculated presence of quartz in assemblages 1 and 3.

Concerning caveat (i), we must consider the non-negligible quantities of ZnO measured in staurolite (Table 1). Assessing our microprobe data, staurolite is the only Zn bearing phase, which is in agreement with other occurrences of Zn-staurolite (e.g. Fox, 1971; Griffen, 1981; Guidotti, 1970; Tuisku et al., 1987). Even with the uniqueness of assemblage 1 of this study (St, Cld, Ms, Pg ± Qz) as well as the apparent lack of zoning, the range of P and T varies somewhat considerably when adjusting the existing thermodynamic data of staurolite endmembers in the thermodynamic database for Zn (Figures 5a and b). Considering these adjustments, we are able to calculate the new stability fields taken as a whole at 1.6 ± 0.2 GPa and 585 ± 20 °C (Figure 7b). Few authors have investigated the effects of ZnO within staurolite, and similarly reported its large influence on a metamorphic stability field (e.g. Fox, 1971; Holdaway et al., 1991; Tuisku et al., 1987). Considering Zn's large influence on the P and T range of stability, treating it as an additional component in staurolite is important (Tuisku et al., 1987). The approach presented here is a suitable way of dealing with Zn-staurolite in the absence of experimentally constrained end-member thermodynamic data and where staurolite is the only Zn bearing phase. The two model calculations (ideal molecular and site mixing) give reasonable bounds on the effect of Zn on the staurolite stability. Although not correlated with Zn content, Li-bearing staurolites have also been demonstrated to expand its stability field (e.g. Dutrow et al., 1986). However, we have not analyzed Li in staurolite.

Concerning caveat (ii), one result from the calculations for assemblage 1 and 3 (Figures 7a, b and c) is the presence of quartz predicted in the stability field. Quartz modal abundance ranges from 1.0-0.1% with increasing P, T and Si content of phengite (Figures 7a and b). However, after detailed microscope investigations and microprobe analysis of several pseudomorph domains from different samples we have not observed quartz associated with chloritoid and staurolite

assemblages. This could be due to the very low proportions of quartz predicted (< 1%) and the statistical chances of cutting a sample in order to observe quartz. Most likely there are two explanations for the predicted quartz: (1) white mica is an abundant phase and the K-Na exchange mixing model may be unreliable, thus Si in paragonite may not be accounted for, and (2) the garnet bearing assemblages surrounding the pseudomorphs containing staurolite + chloritoid are observed to have quartz (Figures 5a and b), hence staurolite + chloritoid assemblages are most likely quartz saturated (or approaching quartz saturation).

6.3 Tectono-metamorphic history of the metapelite

Figure 8 outlines the schematic geological history recorded in the metapelitic lithologies of the Monte Rosa. (a) Variscan HT-LP orogenesis, overprinting metapelitic lithologies and the formation of 1st generation garnets. (b) Intrusion of Variscan-age granite bodies, resulting in local migmatization and a contact metamorphic aureole forming andalusite. (c) Peak Alpine high-P imprint over contact metamorphic andalusite resulting in staurolite-chloritoid within former andalusite pseudomorphs, and 2nd generation garnet bearing assemblages. (d) Late Alpine deformation of the basement locally producing greenschist lithologies.

6.4 Pressure variations and geodynamic implications

Figure 9a shows a comparison of the results of this study with the results from Luisier et al. (2019). When comparing the peak metamorphic conditions of metapelites from this study at 1.6 ± 0.2 GPa, with the peak metamorphic conditions of the whiteschist at 2.2 ± 0.2 GPa and the host metagranite at 1.4 ± 0.2 GPa, the metapelite and metagranite show a consistent peak P, within error, while the whiteschist shows a considerably higher peak P. Even with a conservative estimate (including the error range introduced via Zn-staurolite reduced activity), differences in peak P between metapelite and whiteschist are ~ 0.6 ± 0.2 GPa. Peak T of approximately 550-600 °C for the metagranite was estimated by Luisier et al. (2019) from the whiteschist pseudosection results. Assuming that the staurolite is a reliable thermometer (see staurolite-in line of Figure 5a), we are able to adjust the metagranite peak T estimates of Luisier et al. (2019) to our calculated temperatures of 585 ± 20 °C. Consequently, the data indicates that metagranite, metapelite and whiteschist assemblages exhibit the same peak T, within error. (Luisier et al., 2019).

There are two end-member interpretations for the geodynamic evolution of the Monte Rosa nappe, namely an interpretation based on lithostatic pressure (Figure 9b) and one based on tectonic pressure variations (Figure 9c). For the lithostatic interpretation, the peak P of the

whiteschist indicates a burial depth of the Monte Rosa nappe of ~ 80 km (using 2.35 GPa as peak P and assuming an overburden with an average density of 3000 kg/m^3). Consequently, all peak P estimates for the metagranite and metapelite must be considered as totally unreliable, because all lithologies were at approximately the same burial depth (no tectonic mélange; see section 2.3). In this scenario, the Monte Rosa nappe would have been most likely exhumed exclusively due to buoyancy forces (e.g. Butler et al., 2013; Butler et al., 2014).

We do not favor the lithostatic interpretation, because peak P estimates for metagranite and metapelite are consistent, within error, although the mineral assemblages are considerably different (Figure 9a). Also, the peak T estimates coincide with estimates for the whiteschist. Moreover, a characteristic structural feature of rocks exhumed by buoyancy in a subduction channel, under approximately lithostatic conditions, should be the formation of a tectonic mélange whereby rocks from different depths, having different peak P and T, are mixed inside the same tectonic units (Gerya and Stöckhert, 2006; Roda et al., 2012); but the studied region is not a mélange. For the tectonic pressure interpretation, peak P of the metagranite and metapelite indicate regional peak P of the Monte Rosa nappe whereas the peak P of the whiteschist indicates local pressure variations with pressures higher than the corresponding lithostatic value. Mechanically, such locally higher pressures could be due to compressional stress during the continental collision of the Alpine orogeny, or due to reaction-induced stresses due to volume changes during whiteschist formation (e.g. Luisier et al, 2019). We suggest that the higher pressure in the whiteschist was due to a combination of compressional and reaction-induced stresses. The ~ 1.6 GPa peak P of the entire Monte Rosa nappe is compatible with the orogenic wedge model in which nappe stacking is due to a combination of buoyancy and compressive forces involving accretion, or underplating, during progressive subduction of mainly the European lower crust and mantle (e.g. Escher and Beaumont, 1997; Platt, 1986). Furthermore, Manzotti et al. (2018) recently estimated peak metamorphic conditions for the two main sub-units of the neighboring Gran Paradiso massif (Figure 1), the Gran Paradiso and Money units, and dated the peak metamorphism. They obtained 1.8-2.0 GPa and 500-520 °C for the Gran Paradiso unit, and 1.7-1.8 GPa and ~ 550 °C for the Money unit; dated both at the same age of c. 42 Ma. The peak metamorphic conditions and age of the Gran Paradiso tectonic units are, hence, close to the peak metamorphic conditions of 1.6 ± 0.2 GPa and 585 ± 20 °C (and their age of 42.6 ± 0.6 Ma; (Lapen et al., 2007)), which are representative for the Monte Rosa nappe. We consider this similarity in

peak metamorphic conditions of the two neighboring internal crystalline massifs (Figure 1a) as further support for the feasibility of our proposed peak values.

7 CONCLUSIONS

For the western portions of the Monte Rosa nappe, we have further constrained the metamorphic conditions associated with peak Alpine activity within the Western Alps from metapelitic lithologies. A unique staurolite-chloritoid bearing assemblage was petrologically and thermodynamically investigated resulting in an Alpine peak pressure of 1.6 ± 0.2 GPa and a peak temperature of 585 ± 20 °C. Comparing these results with the peak pressure variations of 0.8 ± 0.3 GPa previously reported in metagranite lithologies, between whiteschist and metagranite, large peak pressure disparities of 0.6 ± 0.2 GPa persist (Figure 9). We rule out explanations for an apparent variability in pressure, such as sluggish kinetics in the metapelites or tectonic mixing, and further highlight the possible existence of mechanically- and/or reaction-induced pressure differences.

Based on our new data and previously published results, we propose that the maximum burial depth of the Monte Rosa unit was likely significantly less than 80 km, which is a depth estimate based on the lithostatic pressure assumption and the local occurrence of minor volumes of whiteschist exhibiting peak pressure >2.2 GPa. The maximum burial depth of the Monte Rosa unit was presumably less than 60 km, which is a depth compatible with burial and exhumation within an orogenic wedge. We further suggest that special care should be taken when using maximal values from published pressure estimates to reconstruct the burial and exhumation history of the corresponding tectonic unit, particularly, when the maximum pressure estimates are limited to minor volumes within the unit.

ACKNOWLEDGEMENTS

We thank B. Dutrow and an anonymous reviewer for their helpful and constructive reviews. This work was supported by the Swiss National Foundation grant numbers 200021-165756. J.V-H thanks Martin Robyr for assistance during EPMA data acquisition. J.V-H also thanks Evangelos Moulas for helpful discussions and guidance regarding thermodynamic adjustments.

REFERENCES

Bearth, P., 1952. Geologie und petrographie des Monte Rosa. Beitraege zur Geologischen Karte der Schweiz Lf., 96: 1-94.

Bearth, P.P., 1958. Über einen Wechsel der Mineralfazies in der Wurzelzone des Penninikums.

Beltrando, M., Compagnoni, R., Lombardo, B., 2010. (Ultra-) High-pressure metamorphism and orogenesis: an Alpine perspective. Gondwana Research, 18(1): 147-166.

Berman, R., 1990. Mixing properties of Ca-Mg-Fe-Mn garnets. American Mineralogist, 75(3-4): 328-344.

Berman, R.G., 1988. Internally-consistent thermodynamic data for minerals in the system Na2O-K2O-CaO-MgO-FeO-Fe2O3-Al2O3-SiO2-TiO2-H2O-CO2. Journal of petrology, 29(2): 445-522.

Borghi, A., Compagnoni, R., Sandrone, R., 1996. Composite PT paths in the Internal Penninic Massifs of the Western Alps: Petrological constraints to their thermo-mecanical evolution.

Butler, J.P., Beaumont, C., Jamieson, R.A., 2013. The Alps 1: A working geodynamic model for burial and exhumation of (ultra) high-pressure rocks in Alpine-type orogens. Earth and Planetary Science Letters, 377: 114-131.

Butler, J.P., Beaumont, C., Jamieson, R.A., 2014. The Alps 2: Controls on crustal subduction and (ultra) high-pressure rock exhumation in Alpine-type orogens. Journal of Geophysical Research: Solid Earth, 119(7): 5987-6022.

Chopin, C., 1987. Very-high-pressure metamorphism in the western Alps: implications for subduction of continental crust. Philosophical Transactions of the Royal Society of London. Series A, Mathematical and Physical Sciences, 321(1557): 183-197.

Chopin, C., Henry, C., Michard, A., 1991. Geology and petrology of the coesite-bearing terrain, Dora Maira massif, Western Alps. European Journal of Mineralogy, 3(2): 263-291.

Chopin, C., Monié, P., 1984. A unique magnesiochloritoid-bearing, high-pressure assemblage from the Monte Rosa, Western Alps: petrologic and 40 Ar-39 Ar radiometric study. Contributions to Mineralogy and Petrology, 87(4): 388-398.

Dal Piaz, G.V., 2001. Geology of the Monte Rosa massif: historical review and personal comments. Schweizerische Mineralogische und Petrographische Mitteilungen, 81(3): 275-303.

Dal Piaz, G.V., Lombardo, B., 1986. Early Alpine eclogite metamorphism in the Penninic Monte Rosa-Gran Paradiso basement nappes of the northwestern Alps. Geol. Soc. Am. Mem, 164: 249-265.

de Capitani, C., Brown, T.H., 1987. The computation of chemical equilibrium in complex systems containing non-ideal solutions. Geochimica et Cosmochimica Acta, 51(10): 2639-2652.

de Capitani, C., Petrakakis, K., 2010. The computation of equilibrium assemblage diagrams with Theriak/Domino software. American Mineralogist, 95(7): 1006-1016.

Deer, W., Howie, R., Zussman, J., 2013. An introduction to the rock-forming minerals Mineralogical Society of Great Britain and Ireland, London.

Dutrow, B.L., Holdaway, M., Hinton, R., 1986. Lithium in staurolite and its petrologic significance. Contributions to Mineralogy and Petrology, 94(4): 496-506.

Ellis, D., Green, D., 1979. An experimental study of the effect of Ca upon garnet-clinopyroxene Fe-Mg exchange equilibria. Contributions to Mineralogy and Petrology, 71(1): 13-22.

Engi, M., Scherrer, N., Burri, T., 2001. Metamorphic evolution of pelitic rocks of the Monte Rosa nappe. Constraints from petrology and single grain monazite age data. Schweizerische Mineralogische und Petrographische Mitteilungen, 81(3): 305-328.

Escher, A., Beaumont, C., 1997. Formation, burial and exhumation of basement nappes at crustal scale: a geometric model based on the Western Swiss-Italian Alps. Journal of Structural geology, 19(7): 955-974.

Eugster, H.P., 1985. Granites and hydrothermal ore deposits: a geochemical framework. Mineralogical Magazine, 49(350): 7-23.

Ferrando, J., Scambelluri, M., Dal Piaz, G., Piccardo, G., 2002. The mafic boudins of the southern Furgg-Zone, Monte Rosa nappe, NW-Italy: from tholeiitic continental basalts to Alpine eclogites and retrogressed products. 81 Riunione Estiva Soc. Geol. It., Torino: 10-12.

Fox, J., 1971. Coexisting chloritoid and staurolite and the staurolite–chlorite isograd from the Agnew Lake area, Ontario, Canada. Geological Magazine, 108(3): 205-219.

Frey, M., Desmons, J., Neubauer, F., 1999. Metamorphic maps of the Alps. Published by the editors and as enclosure to. Schweizerische Mineralogische und Petrographische Mitteilungen, 79(1).

Gasco, I., Borghi, A., Gattiglio, M., 2011. P–T Alpine metamorphic evolution of the Monte Rosa nappe along the Piedmont Zone boundary (Gressoney Valley, NW Italy). Lithos, 127(1-2): 336-353.

Gerya, T., 2015. Tectonic overpressure and underpressure in lithospheric tectonics and metamorphism. Journal of Metamorphic Geology, 33(8): 785-800.

Gerya, T., Stöckhert, B., 2006. Two-dimensional numerical modeling of tectonic and metamorphic histories at active continental margins. International Journal of Earth Sciences, 95(2): 250-274.

Goffe, B., Chopin, C., 1986. High-pressure metamorphism in the Western Alps: zoneography of metapelites, chronology and consequences. Schweizerische mineralogische und petrographische Mitteilungen, 66(1-2): 41-52.

Griffen, D.T., 1981. Synthetic Fe/Zn staurolites and the ionic radius of IVZn2+. American Mineralogist, 66(9-10): 932-937.

Guidotti, C.V., 1970. The mineralogy and petrology of the transition from the lower to upper sillimanite zone in the Oquossoc area, Maine. Journal of Petrology, 11(2): 277-336.

Hacker, B.R., Gerya, T.V., 2013. Paradigms, new and old, for ultrahigh-pressure tectonism. Tectonophysics, 603: 79-88.

Handy, M.R., Schmid, S.M., Bousquet, R., Kissling, E., Bernoulli, D., 2010. Reconciling plate-tectonic reconstructions of Alpine Tethys with the geological–geophysical record of spreading and subduction in the Alps. Earth-Science Reviews, 102(3-4): 121-158.

Hawthorne, F., Ungaretti, L., Oberti, R., Caucia, F., Callegari, A., 1993. The crystal chemistry of staurolite; I, Crystal structure and site populations. The Canadian Mineralogist, 31(3): 551-532.

Holdaway, M., Dutrow, B., Shore, P., 1986. A model for the crystal chemistry of staurolite. American Mineralogist, 71(9-10): 1142-1159.

Holdaway, M. et al., 1991. A new perspective on staurolite crystal chemistry: Use of stoichiometric and chemical end-members for a mole fraction model. American Mineralogist, 76(11-12): 1910-1919.

Holland, T., 1979. Reversed hydrothermal determination of jadeite-diopside activities. Eos, 60: 405.

Holland, T., Powell, R., 1998. An internally consistent thermodynamic data set for phases of petrological interest. Journal of metamorphic Geology, 16(3): 309-343.

Howie, R., Zussman, J., Deer, W., 1992. An introduction to the rock-forming minerals. Longman.

Huang, W., Wyllie, P., 1974. Melting relations of muscovite with quartz and sanidine in the K2O-Al2O3-SiO2-H2O system to 30 kilobars and an outline of paragonite melting relations. American Journal of Science, 274(4): 378-395.

Hurford, A.J., Hunziker, J.C., Stöckhert, B., 1991. Constraints on the late thermotectonic evolution of the western Alps: evidence for episodic rapid uplift. Tectonics, 10(4): 758-769.

Kell, G., Haar, L., Gallagher, J., 1984. NBS/NRC Steam Tables. Thermodynamic and Transport Properties and Computer Programs for Vapor and Liquid States of Water in SI Units. National Standard Reference Data.

Keller, L., Abart, R., Stünitz, H., De Capitani, C., 2004. Deformation, mass transfer and mineral reactions in an eclogite facies shear zone in a polymetamorphic metapelite (Monte Rosa nappe, western Alps). Journal of Metamorphic Geology, 22(2): 97-118.

King, S.W., 1858. The Italian Valleys of the Pennine Alps: A Tour Through All the Romantic and Less-frequented" vals" of Northern Piedmont, from the Tarentaise to the Gries. J. Murray.

Kurz, W., Froitzheim, N., 2002. The exhumation of eclogite-facies metamorphic rocks—a review of models confronted with examples from the Alps. International Geology Review, 44(8): 702-743.

Lanari, P. et al., 2014. XMapTools: A MATLAB©-based program for electron microprobe X-ray image processing and geothermobarometry. Computers & Geosciences, 62: 227-240.

Lapen, T.J. et al., 2007. Coupling of oceanic and continental crust during Eocene eclogite-facies metamorphism: evidence from the Monte Rosa nappe, western Alps. Contributions to Mineralogy and Petrology, 153(2): 139-157.

Le Bayon, R., de Capitani, C., Frey, M., 2006. Modelling phase–assemblage diagrams for magnesian metapelites in the system K2O–FeO–MgO–Al2O3–SiO2–H2O: geodynamic consequences for the Monte Rosa nappe, Western Alps. Contributions to Mineralogy and Petrology, 151(4): 395.

Li, Z.H., Gerya, T.V., Burg, J.-P., 2010. Influence of tectonic overpressure on *P-T* paths of HP-UHP rocks in continental collision zones: thermomechanical modelling. Journal of Metamorphic Geology, 28(3): 227-247.

Luisier, C., Baumgartner, L., Schmalholz, S.M., Siron, G., Vennemann, T., 2019. Metamorphic pressure variation in a coherent Alpine nappe challenges lithostatic pressure paradigm. Nature communications, 10(1): 1-11.

Mancktelow, N., 1993. Tectonic overpressure in competent mafic layers and the development of isolated eclogites. Journal of Metamorphic Geology, 11(6): 801-812.

Mancktelow, N.S., 1995. Nonlithostatic pressure during sediment subduction and the development and exhumation of high pressure metamorphic rocks. Journal of Geophysical Research: Solid Earth, 100(B1): 571-583.

Mancktelow, N.S., 2008. Tectonic pressure: Theoretical concepts and modelled examples. Lithos, 103(1-2): 149-177.

Manzotti, P. et al., 2018. Exhumation rates in the Gran Paradiso Massif (Western Alps) constrained by in situ U–Th–Pb dating of accessory phases (monazite, allanite and xenotime). Contributions to Mineralogy and Petrology, 173(3): 24.

Marger, K. et al., 2019. Origin of Monte Rosa whiteschist from in-situ tourmaline and quartz oxygen isotope analysis by SIMS using new tourmaline reference materials. American Mineralogist: Journal of Earth and Planetary Materials, 104(10): 1503-1520.

Massonne, H.-J., Schreyer, W., 1987. Phengite geobarometry based on the limiting assemblage with K-feldspar, phlogopite, and quartz. Contributions to Mineralogy and Petrology, 96(2): 212-224.

Massonne, H.-J., Szpurka, Z., 1997. Thermodynamic properties of white micas on the basis of high-pressure experiments in the systems K2O-MgO-Al2O3-SiO2-H2O and K2O-FeO-Al3O3-SiO2-H3O. Lithos, 41(1-3): 229-250.

Molnar, P., Lyon-Caen, H., 1988. Some simple physical aspects of the support, structure, and evolution of mountain belts. Processes in continental lithospheric deformation, 218: 179-207.

Moulas, E. et al., 2019. Relation between mean stress, thermodynamic, and lithostatic pressure. Journal of metamorphic geology, 37(1): 1-14.

Nagel, T., De Capitani, C., Frey, M., 2002. Isograds and P–T evolution in the eastern Lepontine Alps (Graubünden, Switzerland). Journal of Metamorphic Geology, 20(3): 309-324.

Niggli, E., 1960. Mineral-zonen der alpinen Metamorphose in den Schweizer Alpen. Int. geol. Congr. Copenhagen, Rep. 21st Sess. Norden, 13: 132-138.

Niggli, E., 1970. Alpine Metamorphose und Alpine Gebirgsbildung: Fortschr. Miner.

Niggli, E., Niggli, C., 1965. Karten der Verbreitung einiger Mineralien der alpidischen Metamorphose in den Schweizer Alpen (Stilpnomelan, Alkali-Amphibol, Chloritoid, Staurolith, Disthen, Sillimanit). Eclogae Geologicae Helvetiae, 58: 335-368.

Pawlig, S., 2001. Geological evolution of the Monte Rosa: constraints from geochronology and geochemistry of a talc kyanite chloritoid shear zone within the Monte Rosa granite (Monte Rosa nappe, Italian Western Alps), Verlag nicht ermittelbar.

Pawlig, S., Baumgartner, L., 2001. Geochemistry of a talc-kyanite-chloritoid shear zone within the Monte Rosa granite, Val d'Ayas, Italy. Schweizerische mineralogische und petrographische Mitteilungen, 81: 329-346.

Petrini, K., Podladchikov, Y., 2000. Lithospheric pressure-depth relationship in compressive regions of thickened crust. Journal of Metamorphic Geology, 18: 67-77.

Platt, J., 1986. Dynamics of orogenic wedges and the uplift of high-pressure metamorphic rocks. Geological society of America bulletin, 97(9): 1037-1053.

Powell, R., Holland, T., 1993. On the formulation of simple mixing models for complex phases. American Mineralogist, 78(11-12): 1174-1180.

Rao, B., Johannes, W., 1979. Further data on the stability of staurolite, Neues Jahrb. Mineral. Monath, 10: 437-447.

Reinecke, T., 1991. Very-high-pressure metamorphism and uplift of coesite-bearing metasediments from the Zermatt-Saas zone, Western Alps. European Journal of Mineralogy: 7-18.

Reuber, G., Kaus, B.J., Schmalholz, S.M., White, R.W., 2016. Nonlithostatic pressure during subduction and collision and the formation of (ultra) high-pressure rocks. Geology, 44(5): 343-346.

Roda, M., Spalla, M.I., Marotta, A.M., 2012. Integration of natural data within a numerical model of ablative subduction: a possible interpretation for the Alpine dynamics of the Austroalpine crust. Journal of Metamorphic Geology, 30(9): 973-996.

Schenker, F.L. et al., 2015. Current challenges for explaining (ultra) high-pressure tectonism in the Pennine domain of the Central and Western Alps. Journal of Metamorphic Geology, 33(8): 869-886.

Schmalholz, S.M., Duretz, T., Hetényi, G., Medvedev, S., 2019. Distribution and magnitude of stress due to lateral variation of gravitational potential energy between Indian lowland and Tibetan plateau. Geophysical Journal International, 216(2): 1313-1333.

Schmalholz, S.M., Medvedev, S., Lechmann, S.M., Podladchikov, Y., 2014. Relationship between tectonic overpressure, deviatoric stress, driving force, isostasy and gravitational potential energy. Geophysical Journal International, 197(2): 680-696.

Schmalholz, S.M., Podladchikov, Y., 2014. Metamorphism under stress: The problem of relating minerals to depth. Geology, 42(8): 733-734.

Schmalholz, S.M., Podladchikov, Y.Y., 2013. Tectonic overpressure in weak crustal-scale shear zones and implications for the exhumation of high-pressure rocks. Geophysical Research Letters, 40(10): 1984-1988.

Skora, S. et al., 2015. Evidence for protracted prograde metamorphism followed by rapid exhumation of the Zermatt-Saas Fee ophiolite. Journal of Metamorphic Geology, 33(7): 711-734.

Steck, A., Masson, H., Robyr, M., 2015. Tectonics of the Monte Rosa and surrounding nappes (Switzerland and Italy): Tertiary phases of subduction, thrusting and folding in the Pennine Alps. Swiss Journal of Geosciences, 108(1): 3-34.

Tuisku, P., Ruosresuo, P., Häkkinen, A.-M., 1987. The metamorphic behaviour and petrogenetic significance of zinc in amphibolite facies, staurolite-bearing mica schists, Puolankajärvi Formation, Central Finland. Geochimica et Cosmochimica Acta, 51(6): 1639-1650.

Wheeler, J., 2018. The effects of stress on reactions in the Earth: sometimes rather mean, usually normal, always important. Journal of Metamorphic Geology, 36(4): 439-461.

Whitney, D.L., Evans, B.W., 2010. Abbreviations for names of rock-forming minerals. American mineralogist, 95(1): 185-187.

SUPPORTING INFORMATION

Appendix S1. Field observations and chemical data

APPENDIX 1

FE AND MG END-MEMBER CORRECTIONS FOR ZN IN STAUROLITE

Due to the absence of thermodynamic data for Zn-staurolite end-members (Fox, 1971; Holdaway et al., 1986; Holdaway et al., 1991), the experimentally derived thermodynamic activity of available endmembers (i.e. Fe- or Mg-staurolite) must be adjusted. In order to adjust the activity for endmembers for non-negligible Zn values we begin with the general equation of the apparent Gibbs free energy (G) for a single component defined in Theriak/Domino (de Capitani and Petrakakis, 2010):

$$G_i^{T,P} = H_i^{T0,P0} - TS_i^{T0,P0} + \int_{T_0}^{T} Cp_i dT - T\int_{T_0}^{T} \frac{Cp_i}{T} dT + \int_{P_0}^{P} V_i^{T,P0} dP \qquad (1.1)$$

For a single mineral endmember the index $i = 1$. In the case of a multi-component ideal solution, G_{sol} would equal:

$$G_{sol} = G^{mech} + G^{mix} = \sum_{i=1}^{n} x_i G_i + \sum_{i=1}^{n} x_i RT \ln\left(\alpha_i^{ideal}\right) \qquad (1.2)$$

The x_i represent the relative fraction of each component and $\sum_{i=1}^{n} x_i = 1$. The Gibbs energy for the single component of Mg-staurolite ($MgSt$) is:

$$G_{MgSt}^{T,P} = H_{MgSt}^{T0,P0} - TS_{MgSt}^{T0,P0} + \int_{T_0}^{T} Cp_{MgSt} dT - T\int_{T_0}^{T} \frac{Cp_{MgSt}}{T} dT + \int_{P_0}^{P} V_{MgSt}^{T,P0} dP \qquad (1.3)$$

The endmember adjustment for a single component (e.g. $MgSt$ & $x_i = 1$) is performed by modifying $S_{MgSt}^{T0,P0}$ in equation (1.3). For reducing the activity of the pure ($x_i \approx 1$) end-member (e.g. *MgSt*) and due to the presence of Zn (*Zn-MgSt*) we introduce the mixing term (G^{mix} in eq. (1.2) in equation (1.3) and assume that the remaining thermodynamic properties of the Zn-bearing MgSt are identical:

$$G_{Zn-MgSt}^{T,P} \approx H_{MgSt}^{T0,P0} - TS_{MgSt}^{T0,P0} + \int_{T_0}^{T} Cp_{MgSt} dT - T\int_{T_0}^{T} \frac{Cp_{MgSt}}{T} dT + \int_{P_0}^{P} V_{MgSt}^{T,P0} dP + RT \ln\left(\alpha_i^{reduced}\right) \qquad (1.4)$$

For pure St end-members (Zn free), equations (1.4) and (1.3) are equivalent because $\alpha_i^{reduced} = 1$. Instead of explicitly treating the mixing term in the Gibbs energy equation (1.4) we prefer to introduce an "effective" entropy ($S_{eff}^{T0,P0}$) in the Gibbs equation, which includes the mixing term. We thus write:

$$G_{Zn-MgSt}^{T,P} \approx H_{MgSt}^{T0,P0} - TS_{eff}^{T0,P0} + \int_{T_0}^{T} Cp_{MgSt} dT - T\int_{T_0}^{T} \frac{Cp_{MgSt}}{T} dT + \int_{P_0}^{P} V_{MgSt}^{T,P0} dP \qquad (1.5)$$

Equations (1.4) and (1.5) must be equivalent expressions and their difference must, hence, be zero. Subtracting equation (1.4) from (1.5) yields:

$$-TS_{eff}^{T0,P0} + TS_{MgSt}^{T0,P0} - RT\ln\left(\alpha_i^{reduced}\right) = 0 \quad (1.6)$$

which after division by T and rearrangement provides the expression for the "effective" entropy:

$$S_{eff}^{T0,P0} = S_{MgSt}^{T0,P0} - R\ln\left(\alpha_i^{reduced}\right) \quad (1.7)$$

Therefore, the presence of Zn, causing $\alpha_i^{reduced} < 1$, would always increase the total entropy via $S_{eff}^{T0,P0}$ and therefore reduce the $G^{T,P}$ of the mixture.

We do not adjust H^o(Fe-staurolite = -23765364 J·mol^{-1} and Mg-staurolite = -25112909 J·mol^{-1}) within THERIAK-DOMINO after Nagel et al. (2002). $S_{eff}^{T0,P0}$ defines an entropy correction, where $S_{MgSt}^{T0,P0}$ is the entropy for the pure phase after Nagel et al. (2002) (Fe-staurolite = 1005.327 J·mol^{-1}·K^{-1} and Mg-staurolite 905.396 J·mol^{-1}·K^{-1}). For a pure phase, $\alpha_i^{reduced}$ = 1, thus $S_{eff}^{T0,P0} = S_{MgSt}^{T0,P0}$. Due to the site multiplicity of staurolite being 4 (T2, M1 – M4) and the equivalent substitutions being $Fe^{2+} = Mg = Zn$ (e.g. Holdaway et al., 1986) we are able to calculate two potential "*endmember"* mixing models in order to correct the activity of Mg and Fe endmembers. Firstly, a 'molecular mixing' model that assumes components are equivalent to mole fractions, thus a linear mixing model via $\alpha_i^{reduced} = \left(1 - \left(\frac{Zn}{4}\right)\right)$. Where Zn = 0.99 atoms per formula unit (a.p.f.u) (Table 1), the resulting $S_{eff}^{T0,P0}$ for Fe-staurolite is 1007.6911 J·mol^{-1}·K^{-1} and Mg-staurolite 907.7601 J·mol^{-1}·K^{-1}. The second, 'site mixing' model has a dependence on the site multiplicity of staurolite being 4 (Holdaway et al., 1991), thus a highly non-linear dependence via $\alpha_i^{reduced} = \left(1 - \left(\frac{Zn}{4}\right)\right)^4$. Where Zn = 0.99 a.p.f.u. (Table 1), the resulting $S_{eff}^{T0,P0}$ for Fe-staurolite is 1014.7834 J·mol^{-1}·K^{-1} and Mg-staurolite 914.8524 J·mol^{-1}·K^{-1}.

FIGURE CAPTIONS

…/figures /FIGURE_1.png

Figure 1

(a) Simplified tectonic map of the western Alps showing the major tectonic units; adapted from Beltrando et al. (2010). The Monte Rosa area is in the red box. (b) Simplified cross-section through the western Alps highlighting the Penninic + Piemont units and major structural discontinuities; modified from figure. 23 of Steck et al. (2015). For better visibility and to provide a first-order geometry, we have combined several tectonic units, for example, the Pre-Alpine Klippen include the Niesen nappe or the Helvetic-Dauphinois Zone includes the Ultrahelvetics. For a detailed tectonic map and section the reader is referred to Steck et al. (2015).

…/figures /FIGURE_2.png

Figure 2

(a) Simplified geological map of the Monte Rosa nappe modified after Steck et al. (2015) with estimates of peak Alpine metamorphism from multiple studies (represented from high to low pressure); study area in red box. (b) Pressure-temperature plot of Alpine metamorphism, outlining the peak Alpine pressure disparities, modified after Luisier et al. (2019).

…/figures /FIGURE_3.png

Figure 3

Geological map and cross-section of the "Peraz" study area in the western Monte Rosa basement and metagranite, including the location of metapelite samples taken for this study (Red stars). Note the separation of pre-Alpine and late-Alpine schistosity.

…/figures /FIGURE_4.png

Figure 4

Representative field images for the study area and metapelitic samples: (a) outcrop of basement metapelites intruded by metagranites (note aplitic dykes), (b) aplitic dyke of the Permian Monte Rosa metagranite cross-cutting gneisses of the Monte Rosa basement, (c) deformed metapelitic basement showing horizontal pre-Alpine deformation sheared and deformed by vertical late Alpine greenschist facies shear zones, (d) domains of preserved peak Alpine assemblages (mineral abbreviations after Whitney and Evans (2010)).

…/figures /FIGURE_5.png

Figure 5

Representative petrological images for the study area and metapelitic samples: (a) textural and compositional domains for sample 16MR-17 including SEM image of typical assemblage 1 and 3 pseudomorph form, (b) plane polarized light image of sample 16MR17 showing the two generations of garnet (assemblage 2), (c) cross polarized light image of sample 16MR17 showing staurolite-chloritoid bearing assemblage (assemblage 1), (d) plain polarized image of sample 19MR-33 showing chloritoid, white mica and late chlorite (assemblage 3), and (e) SEM image of typical assemblage 2 textures. Mineral abbreviations after (Whitney and Evans, 2010).

…/figures /FIGURE_6.png

Figure 6

Normalized mineral chemical data for assemblages 1, 2 and 3 (sample 16MR-17 and 19MR-33): (a) Si in phengites against Al tetrahedral site, (b) chloritoid Mg and Fe-total, (c) Na in paragonite and K in phengite mixing gap of white micas, and (d) ternary plot for garnet compositions in assemblage 2, and ternary plot for staurolite compositions in assemblage 1 (note non-negligible Zn).

…/figures /FIGURE_7.png

Figure 7

Thermodynamic pseudosection modelling for assemblages 1, 2 and 3 (sample 16MR17 and 19MR33) using the Theriak/Domino software and JUN92 Berman database (Berman, 1988): (a) assemblage 1 results in NKFMASH with reduced activity for Mg-Fe endmember solutions based on molecular mixing assumption (a.p.f.u isopleths for Si in phengite), (b) assemblage 1 results in NKFMASH with reduced activity for Mg-Fe endmember solutions based on site mixing assumption (a.p.f.u isopleths for Si in phengite), (c) assemblage 2 results in NCKFMASH (a.p.f.u isopleths for Si in phengite, X paragonite and phengite vol%), and (d) assemblage 3 results in NKFMASH system (a.p.f.u. isopleths for kyanite vol%).

…/figures /FIGURE_8.png

Figure 8

Schematic geological evolution of the polymetamorphic basement of Monte Rosa nappe: (a) Variscan high temperature-low pressure orogenic imprint, defined in this study as large 1st generation garnets at 330 Ma (Engi et al., 2001), (b) intrusion of post-Variscan aged granite bodies (Pawlig and Baumgartner, 2001), associated dykes and associated contact metamorphic aureole most likely forming andalusite grade contact metapelites and late magmatic overprint by Na-saturated hydrothermal alteration, (c) HP imprint during Alpine orogenesis pseudomorphing after andalusite, forming the assemblages investigated in this study, (d) late Alpine deformation associated with decompression to greenschist facies grade.

…/figures /FIGURE_9.png

Figure 9

(a) Final PT results of metapelite samples and comparison of results with whiteschist assemblages and metagranite of Luisier et al. (2019): (b) hypothetical clockwise P-T-depth loop for the Monte Rosa nappe, peak pressure equating to deepest burial of unit using the lithostatic depth assumption, (c) hypothetical clockwise P-T loop for the Monte Rosa nappe where the metagranite and metapelites represent the regional peak pressure in the nappe and the whiteschist represents a local and volumetrically minor area of relatively higher pressure ΔP, potentially caused by mechanical- or reaction-induced stress.

TABLE CAPTIONS

…/tables/TABLE_1.pdf

Table 1 Representative microprobe analysis (16MR-17 and 19MR-33).

SUPPORTING INFORMATION

Appendix S1. Field observations and chemical data

Figure S1. Field image of typical migmatitic textures in the Monte Rosa metapelites in close proximity to metagranite bodies

Figure S2. Field image of late Alpine folding in the metapelitic basement. Preserving early Alpine assemblages in the fold hinge.

Figure S3. Field image of earl Alpine high pressure assemblages pseudomorphing contact metamorphic textures

Figure S4. Mineralogical and textural overview of samples 16MR-17.

Table 1. Representative microprobe analysis (16MR-17 and 19MR-33)

	Assemblage 1				Assemblage 2						Assemblage 3		
Analysis	**Phengite**	**Paragonite**	**Chloritoid**	**Staurolite**	**Phengite**		**Paragonite**	**Garnet**		**Chlorite**	**Phengite**	**Paragonite**	**Chloritoid**
					Core	**Rim**		**Core**	**Rim**				
SiO_2	48.65	47.11	24.96	28.19	50.05	48.02	46.28	37.51	37.11	25.86	47.52	47.59	24.12
Al_2O_3	32.44	40.01	42.10	52.91	28.50	31.84	40.01	20.83	20.86	21.59	34.63	40.85	42.69
TiO_2	0.25	0.08	0.11	0.33	0.18	0.25	0.05	0.41	0.02	0.08	0.57	0.04	0.01
MnO	0.03	0.00	0.00	0.03	0.00	0.00	0.01	1.50	0.59	0.05	0.01	0.00	0.10
ZnO	0.03	0.00	0.00	4.74	0.00	0.02	0.00	0.00	0.02	0.11	0.02	0.00	0.08
FeO	1.35	0.26	20.40	9.59	1.70	1.27	0.33	30.54	36.49	20.10	1.59	0.61	22.94
MgO	2.05	0.10	5.32	1.81	3.21	2.18	0.08	2.72	3.50	18.27	1.20	0.08	3.90
Na_2O	0.96	7.14	0.01	0.09	0.48	0.86	7.07	0.00	0.011	0.01	1.32	7.08	0.00
CaO	0.00	0.13	0.00	0.01	0.00	0.00	0.42	6.74	1.41	0.01	0.02	0.06	0.01
K_2O	9.70	1.11	0.10	0.01	10.43	10.08	0.69	0.01	0.01	0.06	9.58	0.70	0.01
F	0.25	0.04	-	-	-	-	-	-	-	-	-	-	-
Cl	0.01	0.00	-	-	-	-	-	-	-	-	-	-	-
Total	95.71	95.97	93.00	97.71	94.55	94.52	94.56	100.29	100.04	86.13	96.45	97.01	93.86
Normalized*	11 (a)	11 (a)	8 (a)	25.55 (c)**	11 (a)	11 (a)	11 (a)	12 (a)	12 (a)	13 (a)	11 (a)	11 (a)	8 (a)
Si^{4+}	3.22	2.99	2.00	7.95	3.36	3.21	2.98	2.99	2.99	2.51	3.12	2.98	1.94
Al^{3+}	2.53	2.99	3.98	17.58	2.25	2.51	3.03	1.96	1.98	2.47	2.68	3.02	4.04
Ti^{4+}	0.01	0.00	0.00	0.07	0.01	0.02	0.00	0.03	0.00	0.01	0.03	0.00	0.00
Mn^{2+}	0.00	0.00	0.01	0.01	0.00	0.00	0.00	0.10	0.04	0.00	0.00	0.00	0.01
Zn^{2+}	0.00	0.00	0.01	0.99	0.00	0.00	0.00	0.00	0.00	0.01	0.00	0.00	0.01
Fe^{2+}	0.08	0.01	1.37	2.26	0.10	0.08	0.02	2.04	2.46	1.63	0.09	0.03	1.54
Mg^{2+}	0.20	0.01	0.64	0.76	0.32	0.23	0.01	0.32	0.42	2.64	0.12	0.01	0.47
Na^{+}	0.12	0.88	0.00	0.00	0.06	0.11	0.88	0.01	0.00	0.00	0.17	0.86	0.00
Ca^{2+}	0.00	0.01	0.00	0.00	0.00	0.00	0.00	0.58	0.12	0.00	0.00	0.00	0.00
K^{+}	0.82	0.09	0.00	0.00	0.89	0.86	0.06	0.00	0.00	0.01	0.80	0.06	0.00
F	0.00	0.00	-	-	-	-	-	-	-	-	-	-	-
Cl	0.00	0.00	-	-	-	-	-	-	-	-	-	-	-
Total	6.98	6.98	8.01	29.62	6.99	7.02	6.98	8.01	8.01	9.28	7.01	6.96	8.01

* normalization using anions (a) and cations (c)
** normalization after Holdaway et al., (1991)

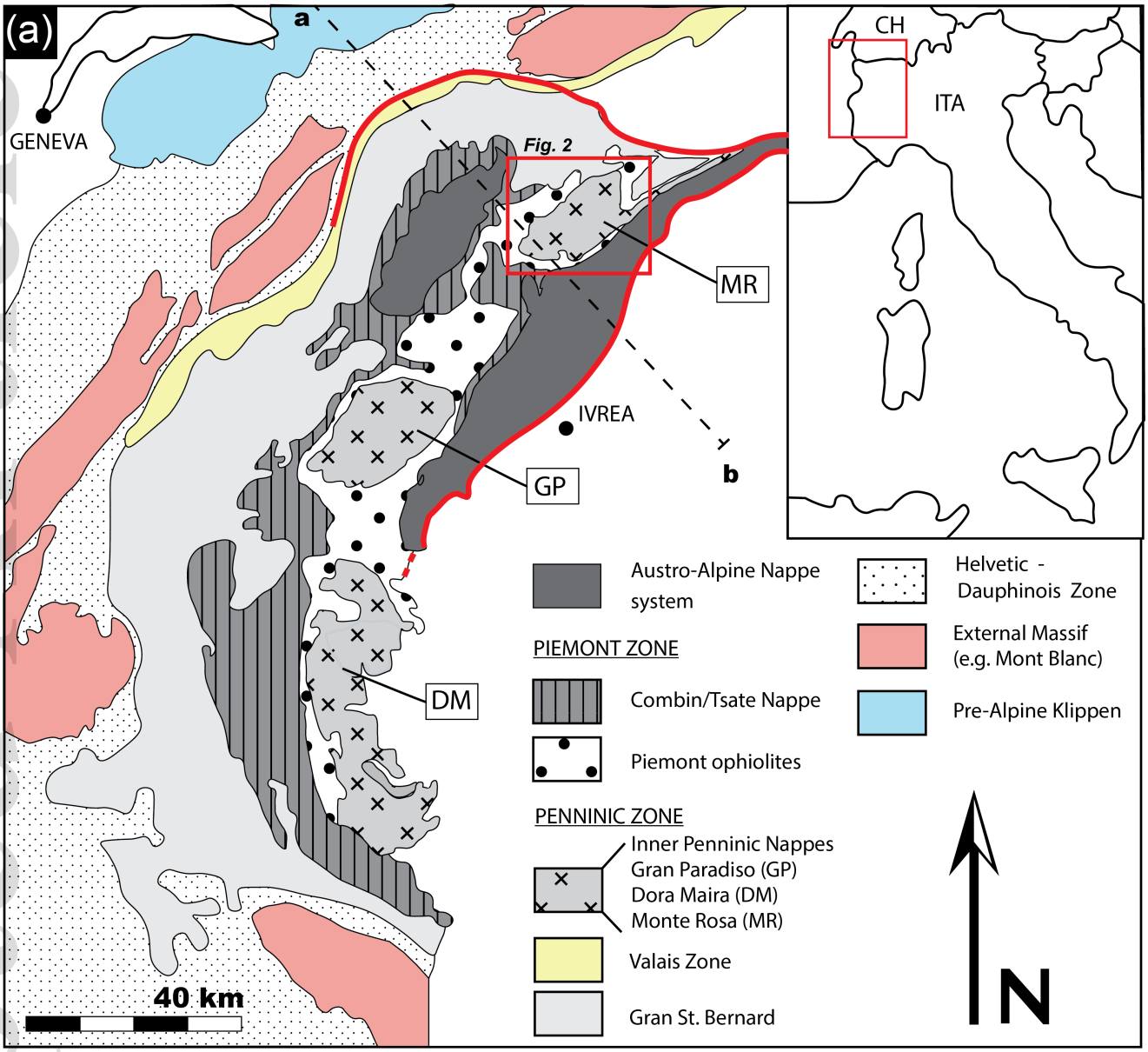

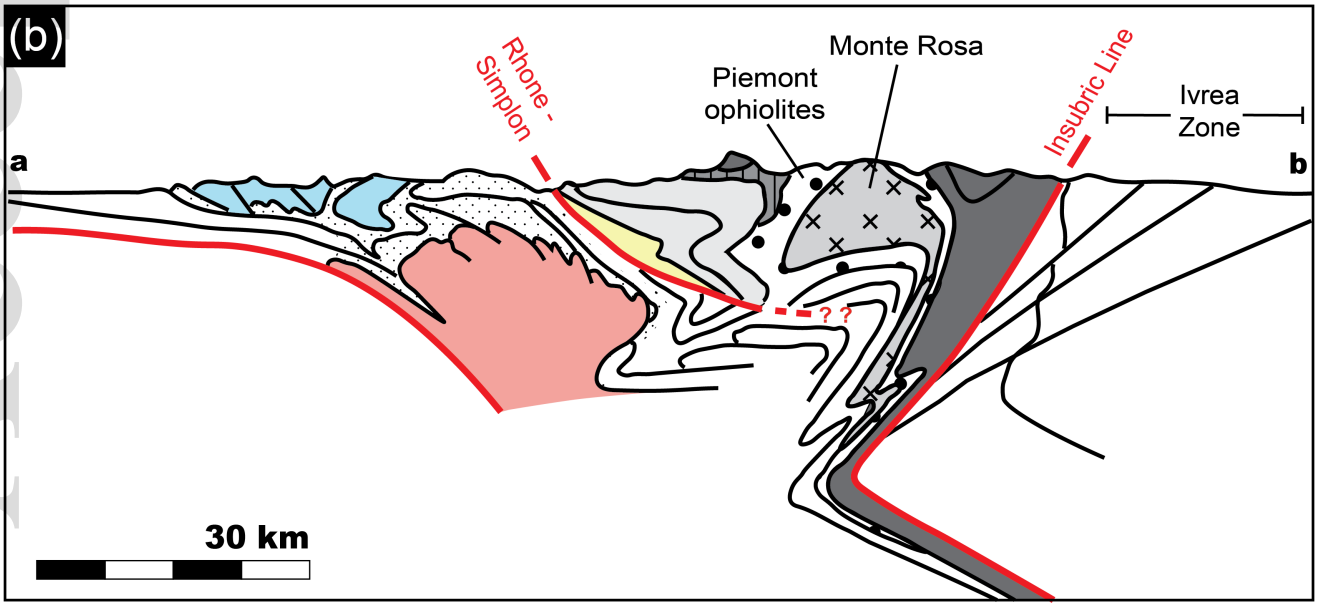

jmg_12595_f1.png

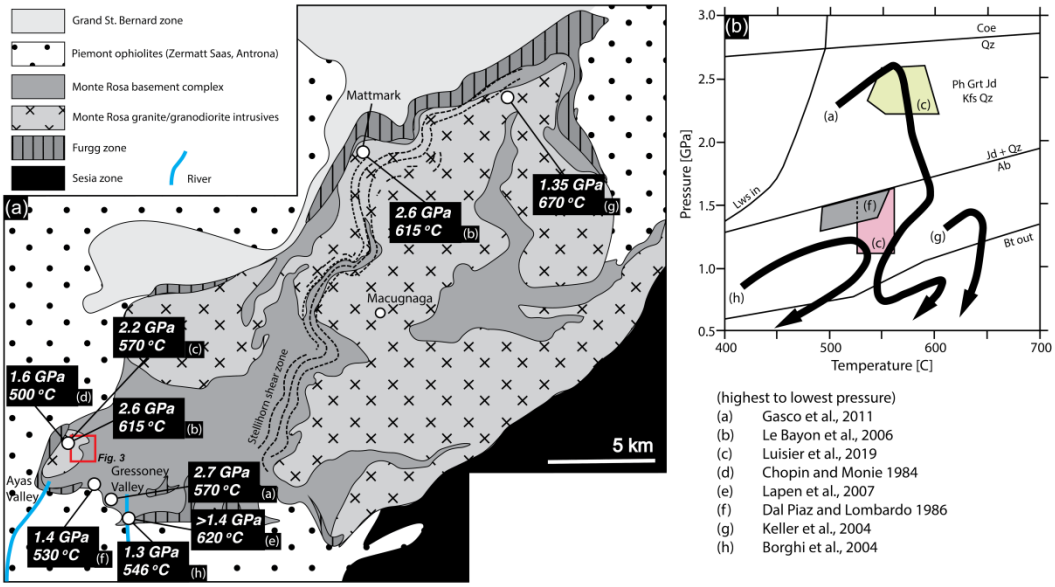

(highest to lowest pressure)
(a) Gasco et al., 2011
(b) Le Bayon et al., 2006
(c) Luisier et al., 2019
(d) Chopin and Monie 1984
(e) Lapen et al., 2007
(f) Dal Piaz and Lombardo 1986
(g) Keller et al., 2004
(h) Borghi et al., 2004

jmg_12595_f2.png

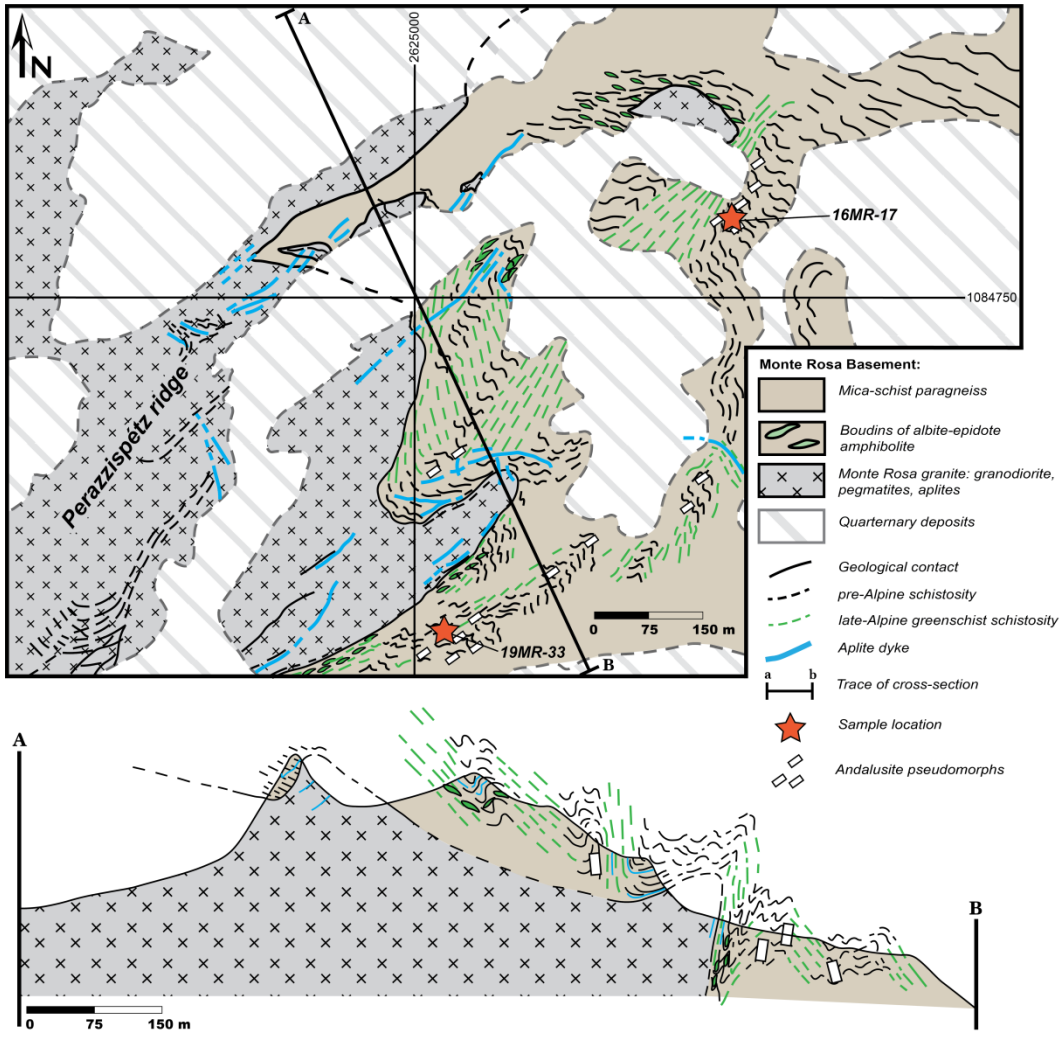

jmg_12595_f3.png

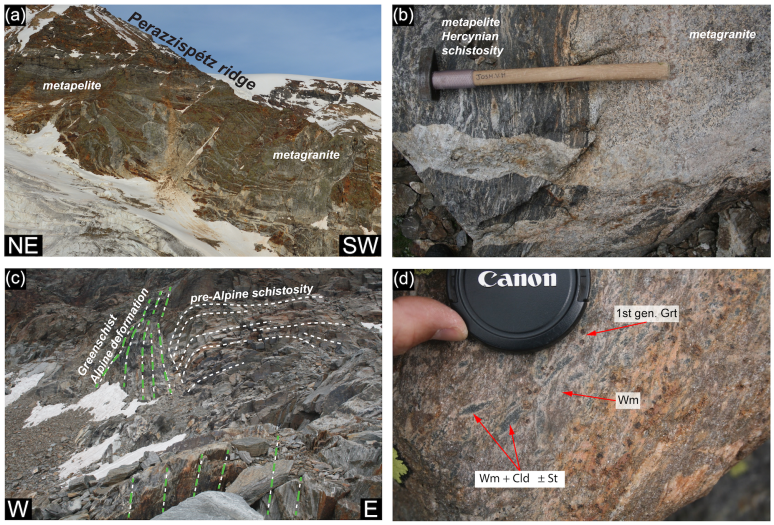

jmg_12595_f4.png

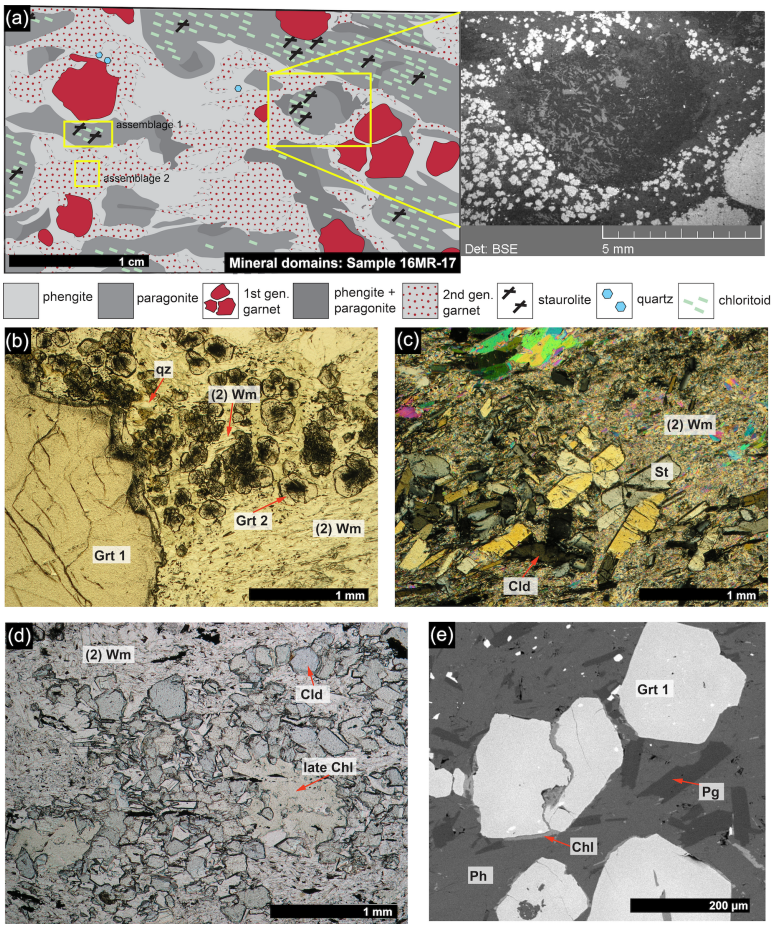

jmg_12595_f5.png

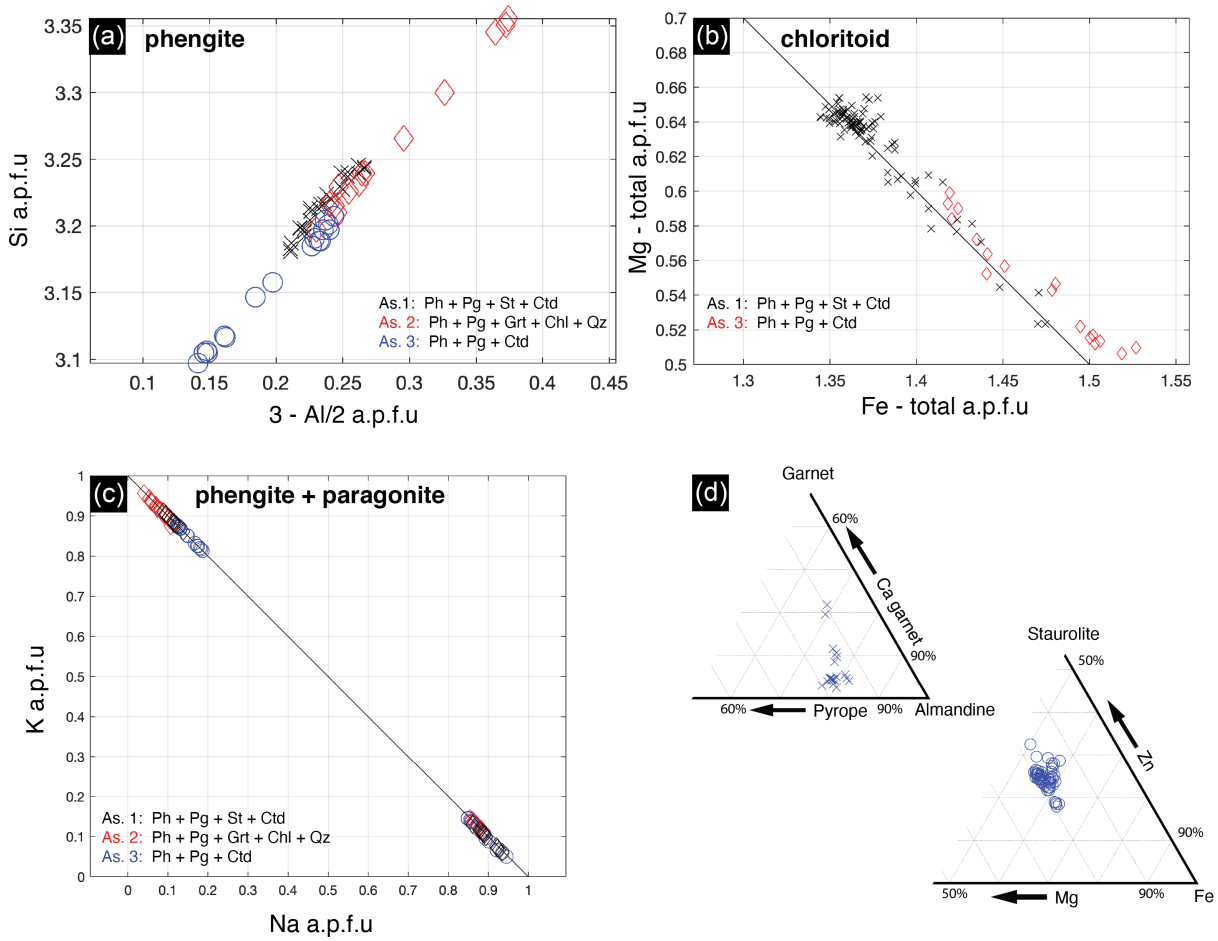

jmg_12595_f6.png

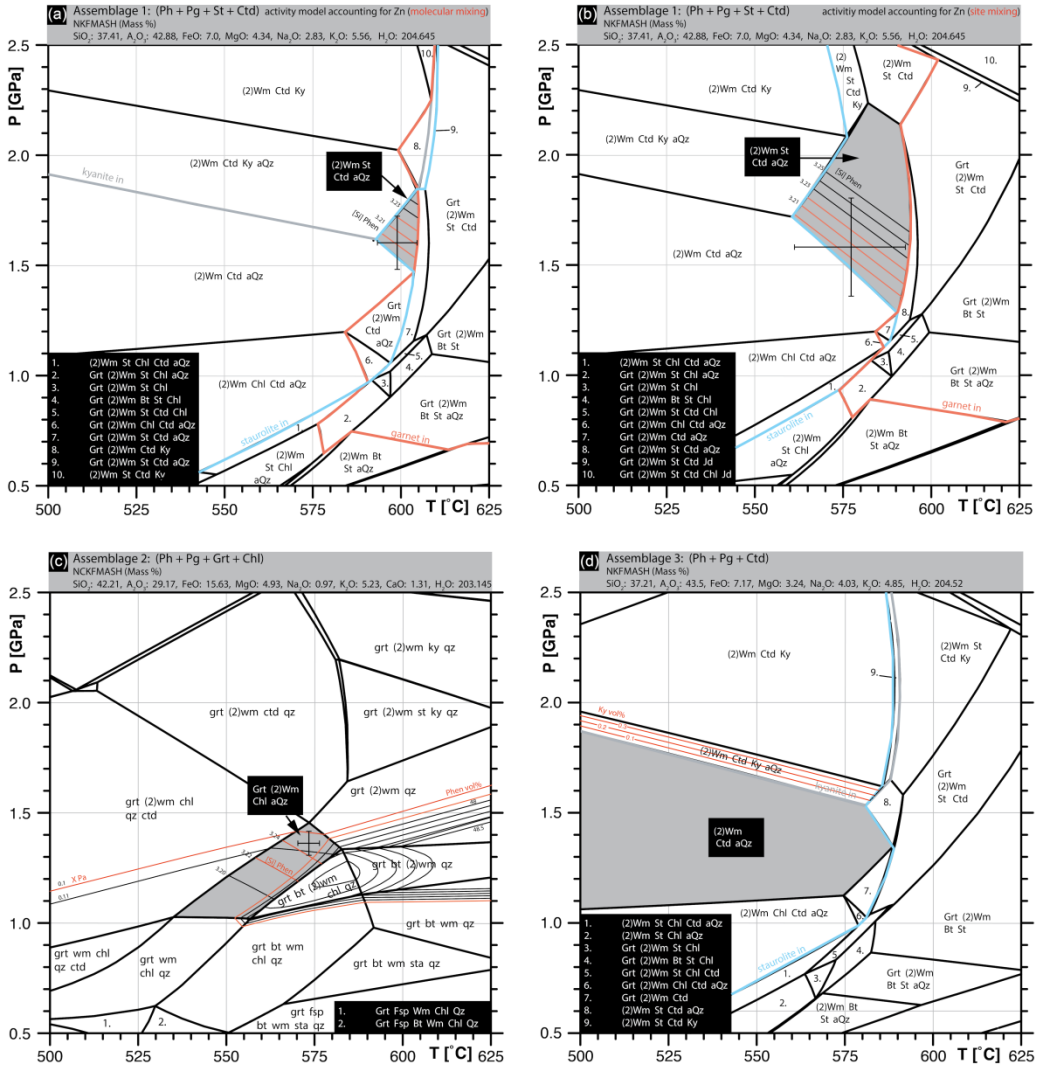

jmg_12595_f7.png

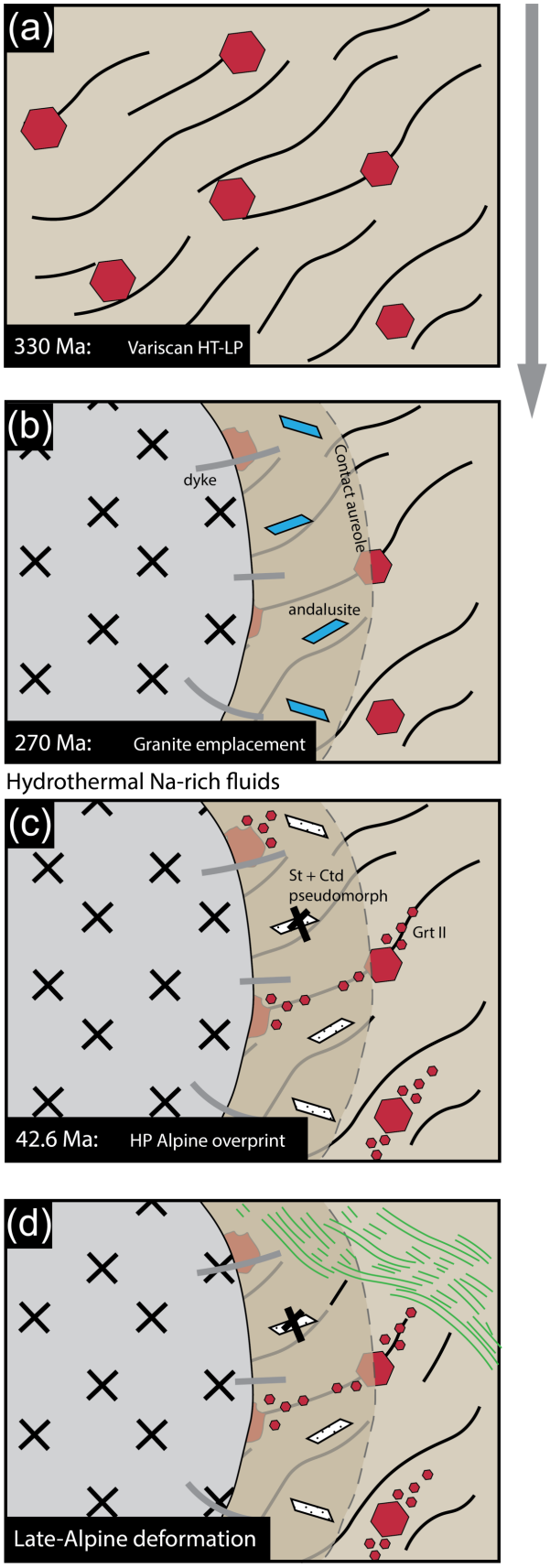

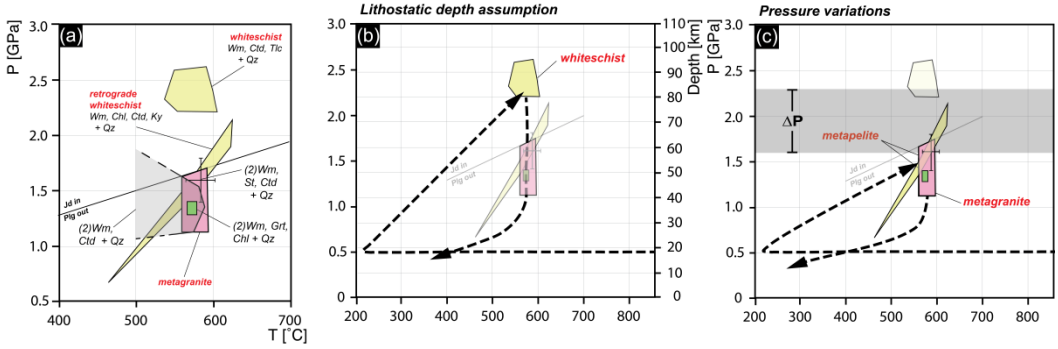

jmg_12595_f9.png